Adropin protects against cardiac metabolic remodeling and dysfunction in HFpEF

Bellina A.S. Mushala[1,2,3], Michael W. Stoner[1,2,3], Janet R. Manning[1,2,3], Paramesha Bugga[1,2,3], Nisha Bhattarai[1,2,3], Maryam Sharifi-Sanjani[1,2,3], Brenda McMahon[1,$], Amber Vandevender[2,4], Steven J. Mullet[7], Brett A. Kaufman[1,2,3], Sruti S. Shiva[1,2,5], Cheng Zhang[6], Eric Goetzman[8], Stephen Y. Chan[1,3], Stacy L. Gelhaus[6,7], Michael J. Jurczak[2,4], and Iain Scott[1,2,3]*

[1]Vascular Medicine Institute, [2]Center for Metabolism and Mitochondrial Medicine, [3]Division of Cardiology, [4]Division of Endocrinology and Metabolism, and [5]Division of Classical Hematology, Department of Medicine, [6]Department of Pharmacology and Chemical Biology, [7]Health Sciences Mass Spectrometry Core, [8]Department of Pediatrics, University of Pittsburgh, Pittsburgh, PA 15261

[$]Current Address: Pierce Hall, Mount Aloysius College, Cresson, PA 16630

*To whom correspondence should be addressed:

Iain Scott, PhD, FAHA, FCVS

Department of Medicine

University of Pittsburgh

BST W1048

200 Lothrop Street

Pittsburgh, PA 15261

iain.scott@pitt.edu

Keywords: Adropin, HFpEF, Mitochondria, Fatty Acid Oxidation, Glucose Oxidation, O-GlcNAcylation

ABSTRACT

Cardiometabolic heart failure with preserved ejection fraction (HFpEF) is a heterogenous metabolic disease, which in the heart presents as left ventricle diastolic dysfunction, ventricular stiffness, and myocardial structural remodeling. Deleterious changes in cardiac metabolism are central to HFpEF pathophysiology, and proposed treatments for the disease have focused on repairing these defects. In this study, we used a preclinical mouse model that recapitulates cardiometabolic HFpEF to elucidate the molecular mechanisms driving cardiac dysfunction, and tested whether recombinant Adropin (a liver- and brain-derived peptide hormone) could reverse observed defects. We show that long-term treatment with Adropin reversed multiple markers of HFpEF-related cardiac dysfunction (including fibrosis, diastolic dysfunction, and cardiomyocyte hypertrophy). Using untargeted metabolomics, we found that Adropin treatment restricted deleterious metabolite entry into the hexosamine biosynthesis pathway, leading to a reduction in the inhibitory O-GlcNAcylation of the cardiac fatty acid oxidation enzyme long chain acyl-CoA dehydrogenase. Our results suggest that Adropin may restore cardiac metabolic function in HFpEF, and that targeting this pathway may be a novel therapeutic avenue for this disease.

INTRODUCTION

Heart failure is a complex clinical syndrome that results from any structural or functional impairments of ventricular filling and/or ejection of blood, and remains the leading cause of morbidity and mortality worldwide (Heidenreich et al., 2023). Heart failure with preserved ejection fraction (HFpEF), a subtype of heart failure, is primarily characterized by cardiac diastolic dysfunction. This presentation of the disease currently accounts for >50% of all heart failure cases, with a global prevalence of approximately 32 million (Shah et al., 2020, Redfield and Borlaug 2023). HFpEF is recognized as a heterogenous syndrome, whose underlying pathophysiological mechanisms include several extracardiac abnormalities such as metabolic derangements, arterial hypertension, microvascular endothelial dysfunction, inflammation, and renal insufficiency (Shah et al., 2016, Shah et al., 2020).

Partly due to a lack of specifically-designed drugs for the disease, treatment for HFpEF currently focuses on the management of comorbidities (e.g. obesity, type 2 diabetes, hypertension), with new guidelines recommending the use of glycemia-reducing therapeutics (e.g. SGLT2 inhibitors) that improve cardiovascular outcomes in heart failure (Kittleson et al., 2023). The recent STEP-HFpEF trial in obesity-related HFpEF demonstrated that therapy-mediated reductions in body weight may also be a key tool in disease regression (Kosiborod et al., 2023). These developments suggest that approaches targeting metabolic defects can offer substantial benefits in this disease. On this basis, we examined whether treatment with recombinant Adropin, a brain- and liver-derived endogenous peptide hormone (Kumar et al., 2008), may have beneficial effects in a preclinical model of cardiometabolic HFpEF.

Previous studies have shown that Adropin improves physical activity (Wong et al, 2014, Ganesh-Kumar et al., 2012), attenuates hepatic steatosis and injury (Kumar et al., 2008, Chen et al., 2019), and reduces vascular stiffness in diet- induced obesity (Jurrissen et al., 2022). In the heart, we recently demonstrated that short-term Adropin treatment can improve cardiac fuel substrate flexibility

by restoring glucose oxidation in the diabetic heart (Thapa et al., 2019b). Combined, these beneficial features raised the question of whether this peptide can be used as a therapeutic intervention in HFpEF. Here, we show that long-term treatment with recombinant Adropin restored cardiac diastolic function, reduced cardiac hypertrophy and fibrosis, and improved whole-body glucose tolerance. These changes were linked to a reversal of metabolic remodeling and improved fatty acid oxidation enzyme activity, suggesting that Adropin treatment mitigates the impact of HFpEF stimuli via improved cardiometabolic function.

MATERIALS AND METHODS

Animal Care and Use

Male C57BL/6J 8-week-old mice were obtained from the Jackson Laboratory and maintained on chow for 4 weeks to acclimate to their new environment. Animals were housed in the University of Pittsburgh animal facility under standard conditions, with *ad libitum* access to water and food, and maintained on a constant 12-hour light/dark cycle. At 12 weeks of age, mice were exposed to normal chow (Chow; 60% carbohydrate, 26% protein, 14% fat; ProLab IsoPro RMH 3000), or a combination of high-fat diet (HFD; 20% carbohydrate, 20% protein, 60% fat; Research Diets D12492) plus N-ω-nitro-L-arginine methyl ester (L-NAME: 0.5 g/L, pH 7.4; ThermoFisher) supplemented in drinking water to induce HFpEF (Schiattarella et al., 2019). After 8 weeks of diet, mice were randomly assigned to a control or treatment group receiving daily intraperitoneal injections of either vehicle or recombinant Adropin (Adr.) at 450 nmol/kg animal weight, prepared in PBS with 0.1% BSA, for the remaining 4 weeks of the study. L-NAME supplemented drinking water was changed weekly, and adropin was made fresh and sterile filtered before each use. Animals were euthanized by isofluorane anesthesia followed by cervical dislocation. Experiments were conducted in compliance with National Institutes of Health guidelines, and followed procedures approved by the University of Pittsburgh Institutional Animal Care and Use Committee.

Echocardiography

Mice were anesthetized using isofluorane (1.5%–2.0% v/v by inhalation) and monitored for cardiac functional parameters in the supine position using a Visual Sonics Vevo 3100. Core temperature was maintained at 37 °C by imaging mice while on a heating pad, and heart rates were kept consistent between experimental groups (~400–500 beats per min). Short axis M-mode was used to assess LV dimensions and motion patterns, pulsed-wave (PW) doppler mode to evaluate blood flow velocities across the mitral valve, and tissue doppler mode to measure mitral annular plane velocity. Doppler profiles were acquired in the parasternal long axis (PLAX) apical 4 chamber view. The left atrial area

was quantified in the apical 4-chamber view by tracing the border of the left atrium. Markers of systolic and diastolic function were calculated using standard echocardiography equations. At the end of the procedure, all mice recovered from anesthesia without difficulties. Image analysis was performed independently by a blinded sonographer, and all parameters were measured at least 3 times with averages presented.

Intraperitoneal Glucose Tolerance Test (IPGTT)

Glucose tolerance tests were performed as previously described with minor modifications (Jurczak et al., 2011). After an overnight fast (~16 h), mice were set-up in restrainers with tails snipped <5mm to prime for blood collection and left to acclimate under a heated bulb for 2 h prior to GTT start time at 9 a.m. Basal plasma samples (t = 0) were collected, and D-glucose was diluted in water (20% final concentration) and sterile filtered for intraperitoneal administration at 1.5 g/kg body weight. Blood glucose was measured by tail bleed at set time points using a Bayer Contour Next EZ handheld glucometer (t = 15, 30, 45, 60, and 120 min).

Histology

Preparation and staining of all histological samples were conducted by the Pitt Biospecimen Core at the University of Pittsburgh. All mice were sacrificed, and tissue harvested for analysis within one hour of completion of the IPGTT study. The apex of the heart was excised from each mouse following euthanasia, fixed in 10% buffered formalin phosphate overnight at shaking incubation, washed 3 times for 5 min with 1X phosphate-buffered saline (PBS), and then transferred to 70% ethanol. Samples were then embedded in paraffin, sectioned into 4 μm slides and stained with hematoxylin and eosin (H&E), wheat germ agglutinin (WGA) or Masson’s Trichrome for analysis. Histology sections were visualized with the Evos FL Auto 2 Microscope, observed changes in structure were quantified using ImageJ software, and representative images are shown.

Transcriptomics

Total RNA was isolated from the left ventricle of the heart using the RNeasy Plus Mini Kit (Qiagen REF 74134). Approximately 2 µg RNA was used for bulk RNA sequencing performed by Azenta/GENEWIZ, based on company recommendations to identify differential gene expression patterns between the experimental groups.

Quantitative Metabolomics

Metabolic quenching and polar metabolite pool extraction was performed by adding ice cold 80% methanol (aqueous) at a ratio of 1:15 wt input tissue:vol. (13C1)-creatinine, (D3)-taurine, (D3)-lactate and (D3)-alanine (Sigma-Aldrich) were added to the sample lysates as an internal standard for a final concentration of 10 µM. Samples are homogenized using an MP Bio FastPrep system using Matrix D (ceramic sphere) for 60 s at 60 hz. The supernatant was then cleared of protein by centrifugation at 16,000 g. Cleared supernatant (2 µL) was subjected to online LC-MS analysis. Analyses were performed by untargeted liquid chromatography-high-resolution mass spectrometry (LC-HRMS). Briefly, samples were injected via a Thermo Vanquish UHPLC and separated over a reversed phase. Thermo HyperCarb porous graphite column (2.1×100 mm, 3 µm particle size) maintained at 55 °C. For the 20 min LC gradient, the mobile phase consisted of the following: solvent A (water/0.1% FA) and solvent B (ACN/0.1% FA). The gradient used was: 0-1 min 1% B, increase to 15% B over 5 min, continue increasing to 98% B over 5 min, hold at 98% B for 5 min, re-equillibrate at 1% B for 5 min. The Thermo IDX tribrid mass spectrometer was operated in both positive and negative ion mode, scanning in ddMS2 mode (2 µscans) from 70 to 800 m/z at 120,000 resolution with an AGC target of $2e^5$ for full scan, $2e^4$ for ms2 scans using HCD fragmentation at stepped 15, 35, 50 collision energies. Source ionization setting was 3.0 and 2.4 kV spray voltage, respectively, for positive and negative mode. Source gas parameters were 35 sheath gas, 12 auxiliary gas at 320 °C, and 8 sweep gas. Calibration was performed prior to analysis using the PierceTM FlexMix Ion Calibration Solutions (Thermo Fisher Scientific). Integrated peak areas were then extracted manually using Quan Browser

(Thermo Fisher Xcalibur ver. 2.7). Untargeted differential comparisons were performed using Compound Discoverer 3.0 (Thermo Fisher) to generate a ranked list of significant compounds with tentative identifications from BioCyc, KEGG, and internal compound databases. Purified standards were then purchased and compared in retention time, m/z, along with ms2 fragmentation patterns to validate the identity of significant hits.

Protein Isolation and Immunoblotting

Heart tissues were rapidly harvested following euthanasia, weighed, RV discarded, and LV flash-frozen in liquid nitrogen. For protein isolation, tissues were minced and lysed in CHAPS buffer (1% CHAPS, 150 mM NaCl, 10 mM HEPES, pH 7.4) using a VWR 4-Place Mini Bead Mill, then incubated on ice for ~ 2.5 h. Homogenates were spun at 10,000 g at 4 °C for 10 min, and the supernatants collected for immunoblotting. For immunoblotting, protein lysates were quantitated using a BioDrop µLITE Analyzer, prepared in LDS sample buffer, separated using Bolt SDS-PAGE 4–12% or 12% Bis–Tris Plus gels, and transferred to nitrocellulose membranes (all Invitrogen). Membranes were blocked using SuperBlock (PBS) Blocking Buffer and incubated overnight in the following primary antibodies: mouse O-GlcNAc (9875), rabbit GFAT (D12F4), rabbit OGT (D1D8Q), rabbit OGA (E9C5U), rabbit GAPDH (2118S) from Cell Signaling Technologies; rabbit CD36 (18836-1-AP), rabbit LCAD (17526-1-AP) from Protein Tech, and GCN5L1 as previously reported (Scott et al., 2012). Protein loading was confirmed using GAPDH as a loading control. Fluorescent anti-goat or anti-rabbit secondary antibodies (red, 700 nm; green, 800 nm) from LiCor were used to detect expression levels. Images were obtained using Licor Odyssey CLx System and protein densitometry was measured using the LiCor Image Studio Lite Ver. 5.2 Software.

Co-Immunoprecipitation

For co-immunoprecipitation experiments, protein lysates were harvested in CHAPS lysis buffer (1% CHAPS, 150 mM NaCl, 10 mM HEPES, pH 7.4), and 500 µg of protein was incubated overnight at 4

°C with 5 µL mouse O-GlcNAc antibody (Cell Signaling). Immunocaptured proteins were isolated using Protein-G and Protein-A agarose beads (Cell Signaling Technology, catalog number 9007), washed 5 times with 500 µL 1% CHAPS buffer, and then eluted in LDS sample buffer (Life Technologies) at 95 °C. Samples were separated on 4-12% Bis–Tris Bolt gels, transferred to nitrocellulose membranes, and probed with appropriate antibodies. Images were obtained using LiCor Odyssey CLx System and protein densitometry was measured using the LiCor Image Studio Lite Ver. 5.2 Software.

Biochemical Assays

To assess the activity of long chain acyl-CoA dehydrogenase enzymes (LCAD), homogenized protein samples were incubated with palmitoyl-CoA as described previously (Thapa et al., 2017). Briefly, ~10 µg of protein was incubated with 0.1 M potassium phosphate, 50 µM 2,6- dichlorophenolindophenol, 2 mM phenazine ethosulfate, 0.2 mM N-ethylmaleimide, 0.4 mM potassium cyanide, and 0.1% Triton X-100 at 37 °C for 4 min. The reaction was initiated with 60 µM palmitoyl-CoA, and the rate of absorbance change was measured/observed at 600 nm over 45 min. Activities were converted to moles of substrate oxidized/min/mass of protein. *In vitro* LCAD activity was measured after incubating a reaction mixture of 4 µg of recombinant LCAD, 0.8 mM UDP-GlcNAc (Sigma, Catalog # U4375), 40 µg/mL of recombinant human O-GlcNAc Transferase (rhOGT) (Catalog # 8446-GT) in assay buffer (25 mM Tris, 10 mM CaCl2, pH 7.5 and 10 mM MgCl2) at 37 °C for 30 min.

Statistics

Means ± SEM were calculated for all data sets. Data were analyzed using one-way ANOVA with Tukey's post-hoc testing to determine differences between genotypes and feeding/treatment groups. Time course data was analyzed using one-way ANOVA with Sidak's post- hoc testing. $P \leq 0.05$ was considered statistically significant. Statistical analyses were performed using GraphPad Prism 9.5 Software.

RESULTS

Circulating Adropin levels are diminished in HFpEF patients

Circulating Adropin levels are known to decrease in patients with type 2 diabetes (Soltani et al, 2023), aging (Yang et al, 2018), and hypertension (Gulen et al, 2016). While these are all comorbidities for HFpEF, there have been no published studies examining circulating Adropin levels in patients with this disease. We therefore measured plasma levels of Adropin in deidentified age- and gender-matched control and HFpEF patient samples (n = 19-20) obtained from a University of Pittsburgh biobank **(Sup. Table 1)**. Consistent with the studies in comorbid disease states, there was a significant decrease in plasma Adropin levels in HFpEF patients relative to non-affected controls **(Fig. 1)**. These data suggest that a reduction in circulating Adropin levels may be linked to HFpEF disease development or progression.

Recombinant Adropin treatment prevents cardiac dysfunction in a mouse model of HFpEF

The potential link between reduced circulating Adropin and HFpEF in patients supported the premise that therapeutic restoration of Adropin levels may be protective against the disease. We therefore used a recently developed two-hit mouse model of HFpEF (Schiattarella et al, 2019) to test this hypothesis. Male C57BL/6J mice were placed on either a chow (control) or HFpEF (60% high fat diet plus L-NAME-supplemented drinking water) diet for 8 weeks. After 8 weeks, HFpEF mice were randomly given either vehicle (PBS) or Adropin (450 nmol/kg/day; Thapa et al, 2019b) by intraperitoneal (I.P.) injection once daily for 4 weeks **(Fig. 2A)**. Daily Adropin treatment significantly increased circulating Adropin levels in HFpEF mice (15.9 vs. 2.2 ng/mL, P = 0.0067), demonstrating that administration of recombinant Adropin could restore plasma concentrations to those observed in healthy humans **(Fig. 1)**.

The recent STEP-HFpEF Phase 3 clinical trial showed that the GLP-1 receptor agonist semaglutide improved patient-reported outcomes in HFpEF, which was at least partially related to weight loss

(Kosiborod et al, 2023). We therefore first examined whether Adropin treatment promoted weight loss in mice, and found that there was no significant difference in body weight between vehicle- and Adropin-treated HFpEF animals **(Fig. 2B, Sup. Fig. 1A)**. Our group and others have previously shown that short-term Adropin treatment (≤ 3 days) leads to improved whole-body glucose tolerance in diet-induced obese mice (Gao et al, 2015; Thapa et al, 2019a). We tested whether long-term Adropin treatment (4 weeks) in HFpEF mice had the same effect, and found that there was a significant decrease in insulin resistance in HFpEF mice treated with Adropin relative to non-treated HFpEF controls **(Fig. 2C, Sup. Fig. 1B)**. Combined, these data suggest that Adropin treatment may have a positive effect on whole-body physiology by reducing glucose intolerance. However, unlike semaglutide in humans, this improvement is unrelated to the beneficial effects of weight loss.

We next examined the effect of Adropin treatment on cardiac functional parameters and tissue structure **(Fig. 2D)**. Mice with HFpEF displayed a significant increase in cardiac weight and a reduction in cardiac output, both of which were absent in Adropin-treated HFpEF mice **(Fig. 2E,F)**. As expected from a HFpEF model, all mouse groups displayed normal systolic function as measured by left ventricular ejection fraction and isovolumetric contraction time **(Fig. 2G, Sup. Table 2)**. While both HFpEF groups displayed a ~25% increase in E/e' ratio, Adropin-treated mice displayed a significant decrease in isovolumetric relaxation time, and a trend towards a decreased E/A ratio relative to untreated HFpEF mice **(Fig. 2H, Sup. Table 2)**. These data indicate that Adropin may increase diastolic function in HFpEF by improving ventricular relaxation, whilst having a more limited impact on left ventricle filling pressures.

Histological analysis of cardiac tissue sections demonstrated that HFpEF mice displayed a significant increase in myocardial interstitial fibrosis and cardiomyocyte cross-sectional area, which was completely reversed following long-term Adropin treatment **(Fig. 2D,I,J)**. The positive impact of Adropin on reducing myocardial fibrosis was evident in bulk RNA-seq analysis or untreated vs.

Adropin-treated HFpEF hearts **(Sup. Table 3)**, with extracellular matrix processes being identified as the top hit in pathway analyses **(Fig. 2K)**. Closer examination demonstrated that multiple genes related to extracellular matrix formation and fibrosis (e.g. *Postn, Fn1, Col1a1*) were significantly downregulated in HFpEF hearts after Adropin treatment **(Fig. 2L, Sup. Fig. 2)**. Combined, these data demonstrate that long-term Adopin treatment in HFpEF promoted whole-body metabolic homeostasis, improved myocardial relaxation, prevented maladaptive cardiac tissue remodeling, and limited cardiomyocyte hypertrophy.

Adropin treatment limits cardiac protein O-GlcNAcylation in HFpEF mice

The decrease in cardiac fibrosis in Adropin-treated HFpEF mice is likely to account for at least some of the functional improvements observed, particularly in terms of myocardial relaxation. However, it is unlikely to explain some of the other improvements that were found to result from Adropin treatment. To better understand the underlying processes involved, we next performed targeted and untargeted metabolomic analyses of hearts from untreated and Adropin-treated HFpEF mice. Surprisingly, there were few significant changes between the hearts of the two HFpEF groups in our targeted analysis of amino acids, energy metabolites, and TCA cycle intermediates **(Sup. Fig. 3)**. In contrast, our untargeted analysis demonstrated that metabolites related to the hexosamine biosynthesis pathway (HBP) were specifically enriched in untreated vs. Adropin-treated HFpEF hearts **(Fig. 3A)**. As the HBP provides substrates for the generation of UDP-GlcNAc, the co-factor for protein O-GlcNAcylation, we next measured the abundance of this posttranslational modification in control and HFpEF hearts.

Immunoblotting using an O-GlcNAc-specific antibody demonstrated that there was a significant increase in cardiac protein O-GlcNAcylation in untreated HFpEF hearts, which was largely reversed (P = 0.06 vs. HFpEF) following long-term Adropin treatment **(Fig. 3B,C)**. O-GlcNAcylation is controlled at the protein level by the rate-limiting enzyme GFAT, and by the opposing activities of the

O-GlcNAc transferase (OGT) and O-GlcNAcase (OGA) which, respectively, add and remove this modification to/from other proteins (e.g., Umapathy et al., 2021, Tran et al., 2020, Prakoso et al., 2022). Unexpectedly, despite the difference in O-GlcNAcylation levels observed in untreated and Adropin-treated HFpEF hearts, there were no significant changes in the abundance of any of these regulatory enzymes **(Fig. 3B,D-F)**.

To determine if changes in HBP substrate abundance, rather that enzyme activity, was controlling the levels of O-GlcNAcylation observed, we examined our metabolomic data for HBP metabolites. Hexose levels in untreated HFpEF mice were significantly increased relative control mice, suggesting that there may be a restriction in glucose moving through the glycolysis pathway **(Fig. 3G)**. Downstream, we observed an accumulation of GlcNAc-6-P, Uridine, and CoA in Adropin-treated HFpEF hearts relative to control and untreated HFpEF mice **(Fig. 3G)**. As these metabolites feed into the HBP at different points, their accumulation suggests a possible reduction of metabolite flux into and through the pathway to generate UDP-GlcNAc, the co-factor for protein O-GlcNAcylation. Combined, these data suggest that part of the function of Adropin in protecting from HFpEF is through its modulatory effect on cardiac protein O-GlcNAcylation.

Adropin-mediated reductions in LCAD O-GlcNAcylation improve its enzymatic activity

Studies in humans and mice have demonstrated that pathways related to cardiac energy metabolism, particularly those in fatty acid utilization, are negatively impacted by HFpEF progression (Tong et al, 2021; Hahn et al, 2023; O'Sullivan et al, 2024). We therefore examined whether specific fatty acid oxidation enzymes were impacted by the increased protein O-GlcNAcylation observed above. Using O-GlcNAc-specific immunoprecipitation we observed that the beta oxidation enzyme long-chain acyl-CoA dehydrogenase (LCAD) displayed elevated O-GlcNAcylation in HFpEF hearts, which was reversed by Adropin treatment **(Fig. 4A,B)**. We examined the effect of O-GlcNAcylation on LCAD enzymatic activity *ex vivo*, and found that its ability to oxidize C16 palmitoyl-CoA was reduced in vehicle-treated HFpEF hearts, but not those

treated with Adropin **(Fig. 4C)**. Combined, there was a significant negative correlation between LCAD O-GlcNAcylation abundance and its enzymatic activity across all cardiac tissues **(Fig. 4D)**, which was unrelated to LCAD protein abundance **(Sup. Fig 4)**. To confirm the regulatory effect of increased O-GlcNAcylation on LCAD activity, we performed a series of *in vitro* assays. LCAD activity was significantly decreased in the presence of the O-GlcNAcylation substrate (UDP-GlcNAc) and transferase enzyme (OGT), but not the substrate alone **(Fig. 4E)**. Finally, we investigated whether changes in lipid handling may be related to the observed decrease in LCAD enzymatic activity, and measured the abundance of the key cardiac lipid droplet membrane protein perilipin-5 (PLIN5). In untreated HFpEF mice there was a significant increase in PLIN5, (suggestive of increased lipid droplet size) compared to control mice, which was absent following Adropin treatment **(Fig. 4F)**. Combined, our data suggests that increased O-GlcNAcylation of fatty acid enzymes like LCAD in HFpEF may decrease their activity and lead to myocardial lipid accumulation, which can be reversed by Adropin treatment.

DISCUSSION

Studies on Adropin signaling in cardiometabolic disease have focused on its effects on fuel energy metabolism, with limited exploration of its role on myocardial structure and function (reviewed in Mushala et al., 2021). Short-term Adropin treatment improved cardiac work and efficiency *ex vivo*, which was accompanied by enhanced insulin signaling in lean mice (Altamimi et al., 2019). In contrast, exposure to a high-fat diet inhibited acute Adropin-driven improvements in contractile function, and insulin stimulation failed to compensate for this impaired cardiac contractility in diet-induced obese mice *ex vivo* (Thapa et al., 2022). In this study, we demonstrate that chronic Adropin treatment *in vivo* restores cardiac function, specifically left ventricular diastolic function, in the failing diabetic myocardium of mice.

Diastolic dysfunction is a hallmark of not only HFpEF, but also diabetic cardiomyopathy (DCM), where relaxation and filling pressure of the left ventricle is impaired (reviewed in Jia et al., 2018). Abnormalities of LV passive elasticity are often caused by structural impediments, such as increased cardiomyocyte diameter and extracellular matrix deposition, which contribute to diastolic dysfunction (Aurigemma et al., 2006). Our data shows that Adropin treatment attenuates LV hypertrophy and fibrosis **(Fig. 2)**, indicative of improved structural remodeling. In addition, transcriptomic analysis demonstrated similar increases in pro-fibrotic pathways as seen in HFpEF patients (Ye et al., 2023) which was attenuated upon Adropin treatment **(Fig. 2)**, providing further evidence of restored myocardial structure and function. Therefore, our findings collectively highlight the therapeutic potential of prolonged Adropin treatment in preventing cardiac remodeling and functional decline in HFpEF and/or DCM.

Data presented in this study add to our growing understanding of the transcriptomic and metabolomic signature of the HFD + L-NAME HFpEF model, providing preclinical evidence of known mechanisms underlying the pathogenesis of cardiometabolic HFpEF in patients, such as fuel substrate inflexibility

(Hahn et al., 2023). Unlike previous acute studies from our group and others, the ability of Adropin treatment to regulate cardiac substrate utilization was independent of the inhibitory effects of PDK4 or GCN5L1 on pyruvate dehydrogenase activity (Thapa et al., 2019b, Altamimi et al., 2019). Instead, we found that Adropin treatment may reduce flux through the HBP, which inhibits cardiac protein O-GlcNAcylation to promote fatty acid oxidation **(Figs. 3,4)**. The HBP is a non-oxidative branch of glycolysis where the rate-limiting enzyme, GFAT, uses fructose-6-phosphate and glutamine to catalyze its conversion into glucosamine-6-phosphate, which is subsequently metabolized through a series of reactions utilizing substrates from major metabolic pathways to generate the end-product UDP-GlcNAc (Figs. 4 and 5, Umapathi et al., 2021). UDP-GlcNAc serves as the co-factor for the attachment of an O-linked β-N-acetyl glucosamine moiety (O-GlcNAc) to serine and threonine residues of nuclear, cytoplasmic, and mitochondrial proteins, using 2-3% of the total cellular glucose found in the heart (Tran et al., 2020).

The dynamic on- and off-cycling of the O-GlcNAc modification is regulated by the activity of two enzymes, O-GlcNAc transferase (OGT) and O-GlcNAcase (OGA), respectively (Prakoso et al., 2022). Several studies have implicated aberrant regulation of the HBP, and consequent maladaptive protein O-GlcNAcylation, in heart failure (e.g., Umapathy et al., 2021, Tran et al., 2020, Prakoso et al., 2022). These studies have identified changes in OGT and OGA enzyme expression as the predominant mechanism that triggers excessive protein O-GlcNAcylation in diabetic hearts. However, here we found that changes in substrate entry from amino acid metabolism (glutamine), fatty acid metabolism (coenzyme A), and nucleotide metabolism (uridine) increased UDP-GlcNAc availability to promote increased cardiac protein O-GlcNAcylation levels **(Fig. 3)**. Notably, previous comparative proteomics studies revealed dysregulated mitochondrial O-GlcNAcylation in diabetic hearts (Ma et al., 2016), with key targets in fatty acid oxidation that have subsequently been linked to increased enzyme activity in pressure-overload hypertrophy (Zhu et al., 2022).

Laczy et al. (2011) showed that increased cardiac O-GlcNAcylation was associated with a decrease in glucose oxidation and a stimulation of fatty acid oxidation *ex vivo*, through increased CD36 expression and O-GlcNAcylation. While we observed a significant increase in CD36 protein abundance, which was significantly attenuated by Adropin treatment **(Sup. Fig. 5)**, direct evidence of O-GlcNAc modification on CD36 was not detected (blots not shown). Instead, we identified the FAO enzyme LCAD as a target of O-GlcNAcylation in HFpEF mice, and Adropin treatment showed moderate inhibition of the modification of these targets **(Fig. 4)**. Interestingly, we found that LCAD O-GlcNAcylation was associated with decreased cardiac enzyme activity in HFpEF mouse hearts, which was restored upon Adropin treatment **(Fig. 4)**. The inhibitory effect of O-GlcNAcylation on LCAD enzyme activity was confirmed *in vitro*, further suggesting that Adropin treatment may augment FAO activity via this mechanism. Further studies need to be conducted to determine whether Adropin-mediated changes of cardiac FAO enzyme O-GlcNAcylation regulates fatty acid utilization in the heart *in vivo.*

Our study has two major limitations. Firstly, the exclusive use of male animals prohibits the investigation into possible sex differences in Adropin-mediated effects observed in the heart. Previous studies using the current HFpEF model have demonstrated that female sex is protective against cardiac dysfunction (Tong et al, 2019). On this basis, our study exclusively examined male mice, and it is unknown whether the findings are relevant for female mice. Epidemiological data show that women display a higher prevalence of diastolic dysfunction (HFpEF) compared to men (Gori et al., 2014, Beale et al., 2018, Duca et al., 2018). Sexual dimorphism in metabolic homeostasis influences the development of cardiac dysfunction (Lindman et al., 2014, Lagou et al., 2021), suggesting a potential role of reproductive hormones in cardiometabolic HFpEF. A recent study showed that sex hormones regulate diastolic performance in C57BL/6J mice, with females displaying an increased susceptibility to the development of HFpEF compared to males, as similarly observed in the clinic, due to mitochondrial dysfunction (Cao et al., 2022). Interestingly, hepatic Adropin production has

been shown to be regulated by estrogen (Stokar et al., 2022), suggesting a potential difference in basal circulating Adropin levels between male and female mice, which may affect their predisposition to HFpEF and consequent response to exogenous adropin treatment. Further work investigating whether Adropin treatment elicits sex-dependent differences in cardiac functional output and substrate use is required to comprehensively characterize its therapeutic potential.

Secondly, our metabolomics data relied on a cross-sectional analysis of HFpEF hearts, which precluded flux measurements of metabolites related to the HBP. While cross-sectional metabolomics data has allowed us to make major advances of our understanding of HFpEF (e.g., Hahn et al, 2023), it does limit our understanding of how metabolite abundance changes in response to disease progression. Future work will likely include the use of stably-labeled isotope tracers for specific metabolites, or the measurement of metabolites entering and exiting the heart (e.g., O'Sullivan et al, 2024), to achieve a better understanding of HBP metabolite flux.

In summary, we found that HFpEF-driven disruptions to normal cardiac energy metabolism led to an apparent shunt of glycolytic intermediates into the HBP, which promoted an increase in cardiac protein O-GlcNAcylation and decreased fatty acid oxidation enzyme activity. Remarkably, long-term Adropin treatment reversed this metabolic remodeling in the heart, leading to restored cardiac structure and diastolic function. These findings are the first to report the long-term effects of Adropin signaling on cardiac function and substrate flexibility in HFpEF, highlighting this pathway as a potential target for future therapeutic interventions.

REFERENCES

Altamimi, T. R., Gao, S., Karwi, Q. G., Fukushima, A., Rawat, S., Wagg, C. S., Zhang, L., & Lopaschuk, G. D. (2019). Adropin regulates cardiac energy metabolism and improves cardiac function and efficiency. *Metabolism: clinical and experimental*, *98*, 37–48.

Aurigemma, G.P., Zile, M.R. & Gaasch, W.H. Contractile behavior of the left ventricle in diastolic heart failure: with emphasis on regional systolic function. Circulation 113, 296- 304 (2006)

Beale, A. L., Meyer, P., Marwick, T. H., Lam, C. S. P., & Kaye, D. M. (2018). Sex Differences in Cardiovascular Pathophysiology: Why Women Are Overrepresented in Heart Failure With Preserved Ejection Fraction. *Circulation*, *138*(2), 198–205.

Cao, Y., Vergnes, L., Wang, Y. C., Pan, C., Chella Krishnan, K., Moore, T. M., Rosa-Garrido, M., Kimball, T. H., Zhou, Z., Charugundla, S., Rau, C. D., Seldin, M. M., Wang, J., Wang, Y., Vondriska, T. M., Reue, K., & Lusis, A. J. (2022). Sex differences in heart mitochondria regulate diastolic dysfunction. *Nature communications*, *13*(1), 3850.

Chen, X., Xue, H., Fang, W., Chen, K., Chen, S., Yang, W., Shen, T., Chen, X., Zhang, P., & Ling, W. (2019). Adropin protects against liver injury in nonalcoholic steatohepatitis via the Nrf2 mediated antioxidant capacity. *Redox biology*, *21*, 101068.

Duca, F., Zotter-Tufaro, C., Kammerlander, A. A., Aschauer, S., Binder, C., Mascherbauer, J., & Bonderman, D. (2018). Gender-related differences in heart failure with preserved ejection fraction. *Scientific reports*, *8*(1), 1080.

Ganesh Kumar, K., Zhang, J., Gao, S., Rossi, J., McGuinness, O. P., Halem, H. H., Culler, M. D., Mynatt, R. L., & Butler, A. A. (2012). Adropin deficiency is associated with increased adiposity and insulin resistance. *Obesity (Silver Spring, Md.)*, *20*(7), 1394–1402.

Gao, S., McMillan, R. P., Zhu, Q., Lopaschuk, G. D., Hulver, M. W., & Butler, A. A. (2015). Therapeutic effects of adropin on glucose tolerance and substrate utilization in diet-induced obese mice with insulin resistance. *Molecular metabolism*, *4*(4), 310–324.

Gori, M., Lam, C. S., Gupta, D. K., Santos, A. B., Cheng, S., Shah, A. M., Claggett, B., Zile, M. R., Kraigher-Krainer, E., Pieske, B., Voors, A. A., Packer, M., Bransford, T., Lefkowitz, M., McMurray, J. J., Solomon, S. D., & PARAMOUNT Investigators (2014). Sex-specific cardiovascular structure and function in heart failure with preserved ejection fraction. *European journal of heart failure, 16(5), 535–542.*

Gulen, B., Eken, C., Kucukdagli, O. T., Serinken, M., Kocyigit, A., Kılıc, E., & Uyarel, H. (2016). Adropin levels and target organ damage secondary to high blood pressure in the ED. *The American journal of emergency medicine, 34(11), 2061–2064.*

Hahn, V. S., Petucci, C., Kim, M. S., Bedi, K. C., Jr, Wang, H., Mishra, S., Koleini, N., Yoo, E. J., Margulies, K. B., Arany, Z., Kelly, D. P., Kass, D. A., & Sharma, K. (2023). Myocardial Metabolomics of Human Heart Failure With Preserved Ejection Fraction. *Circulation*, *147*(15), 1147–1161.

Heidenreich,P.A.,Bozkurt,B.,Aguilar,D.,Allen,L.A.,Byun,J.J.,Colvin,M.M.,Deswal,A., Drazner, M. H., Dunlay, S. M., Evers, L. R., Fang, J. C., Fedson, S. E., Fonarow, G. C., Hayek, S. S., Hernandez, A. F., Khazanie, P., Kittleson, M. M., Lee, C. S., Link, M. S., Milano, C. A., ... Yancy, C. W. (2022).

2022 AHA/ACC/HFSA Guideline for the Management of Heart Failure: A Report of the American College of Cardiology/American Heart Association Joint Committee on Clinical Practice Guidelines. *Circulation*, *145*(18), e895–e1032.

Jia, G., Hill, M. A., & Sowers, J. R. (2018). Diabetic Cardiomyopathy: An Update of Mechanisms Contributing to This Clinical Entity. *Circulation research*, *122*(4), 624–638.

Jurczak, M. J., Lee, H. Y., Birkenfeld, A. L., Jornayvaz, F. R., Frederick, D. W., Pongratz, R. L., Zhao, X., Moeckel, G. W., Samuel, V. T., Whaley, J. M., Shulman, G. I., & Kibbey, R. G. (2011). SGLT2 deletion improves glucose homeostasis and preserves pancreatic beta-cell function. Diabetes, 60(3), 890–898.

Jurrissen, T. J., Ramirez-Perez, F. I., Cabral-Amador, F. J., Soares, R. N., Pettit-Mee, R. J., Betancourt-Cortes, E. E., McMillan, N. J., Sharma, N., Rocha, H. N. M., Fujie, S., Morales-Quinones, M., Lazo-Fernandez, Y., Butler, A. A., Banerjee, S., Sacks, H. S., Ibdah, J. A., Parks, E. J., Rector, R. S., Manrique-Acevedo, C., Martinez-Lemus, L. A., ... Padilla, J. (2022). Role of adropin in arterial stiffening associated with obesity and type 2 diabetes. *American journal of physiology. Heart and circulatory physiology*, *323*(5), H879–H891.

Kittleson, M. M., Panjrath, G. S., Amancherla, K., Davis, L. L., Deswal, A., Dixon, D. L., Januzzi, J. L., Jr, & Yancy, C. W. (2023). 2023 ACC Expert Consensus Decision Pathway on Management of Heart Failure With Preserved Ejection Fraction: A Report of the American College of Cardiology Solution Set Oversight Committee. *Journal of the American College of Cardiology*, *81*(18), 1835–1878.

Kosiborod, M. N., Abildstrøm, S. Z., Borlaug, B. A., Butler, J., Rasmussen, S., Davies, M., Hovingh, G. K., Kitzman, D. W., Lindegaard, M. L., Møller, D. V., Shah, S. J., Treppendahl, M. B., Verma, S., Abhayaratna, W., Ahmed, F. Z., Chopra, V., Ezekowitz, J., Fu, M., Ito, H., Lelonek, M., … STEP-HFpEF Trial Committees and Investigators (2023). Semaglutide in Patients with Heart Failure with Preserved Ejection Fraction and Obesity. *The New England journal of medicine*, *389*(12), 1069–1084.

Kumar, K. G., Trevaskis, J. L., Lam, D. D., Sutton, G. M., Koza, R. A., Chouljenko, V. N., Kousoulas, K. G., Rogers, P. M., Kesterson, R. A., Thearle, M., Ferrante, A. W., Jr, Mynatt, R. L., Burris, T. P., Dong, J. Z., Halem, H. A., Culler, M. D., Heisler, L. K., Stephens, J. M., & Butler, A. A. (2008). Identification of adropin as a secreted factor linking dietary macronutrient intake with energy homeostasis and lipid metabolism. *Cell metabolism*, *8*(6), 468–481.

Laczy, B., Fülöp, N., Onay-Besikci, A., Des Rosiers, C. & Chatham, J.C. Acute Regulation of Cardiac Metabolism by the Hexosamine Biosynthesis Pathway and Protein OGlcNAcylation. PLOS ONE 6, e18417 (2011)

Lagou, V., Mägi, R., Hottenga, J.J. *et al.* Sex-dimorphic genetic effects and novel loci for fasting glucose and insulin variability. *Nat Commun* **12**, 24 (2021).

Lindman, B. R., Dávila-Román, V. G., Mann, D. L., McNulty, S., Semigran, M. J., Lewis, G. D., de las Fuentes, L., Joseph, S. M., Vader, J., Hernandez, A. F., & Redfield, M. M. (2014). Cardiovascular phenotype in HFpEF patients with or without diabetes: a RELAX trial ancillary study. *Journal of the American College of Cardiology*, *64*(6), 541–549.

Ma, J., Banerjee, P., Whelan, S. A., Liu, T., Wei, A. C., Ramirez-Correa, G., McComb, M. E., Costello, C. E., O'Rourke, B., Murphy, A., & Hart, G. W. (2016). Comparative Proteomics Reveals

Dysregulated Mitochondrial O-GlcNAcylation in Diabetic Hearts. *Journal of proteome research, 15(7), 2254–2264.*

Mushala, B. A. S., & Scott, I. (2021). Adropin: a hepatokine modulator of vascular function and cardiac fuel metabolism. *American journal of physiology. Heart and circulatory physiology*, *320*(1), H238–H244.

Prakoso, D., et al. Fine-tuning the cardiac O-GlcNAcylation regulatory enzymes governs the functional and structural phenotype of the diabetic heart. Cardiovascular Research 118, 212-225

O'Sullivan JF, Li M, Koay YC, Wang XS, Guglielmi G, Marques FZ, Nanayakkara S, Mariani J, Slaughter E, Kaye DM. (2024). Cardiac Substrate Utilization and Relationship to Invasive Exercise Hemodynamic Parameters in HFpEF. JACC Basic Transl Sci. 9:281-299

Redfield, M.M., & Borlaug, B.A.(2023).Heart Failure With Preserved Ejection Fraction: A Review. *JAMA*, *329*(10), 827–838.

Schiattarella, G. G., Altamirano, F., Tong, D., French, K. M., Villalobos, E., Kim, S. Y., Luo, X., Jiang, N., May, H. I., Wang, Z. V., Hill, T. M., Mammen, P. P. A., Huang, J., Lee, D. I., Hahn, V. S., Sharma, K., Kass, D. A., Lavandero, S., Gillette, T. G., & Hill, J. A. (2019). Nitrosative stress drives heart failure with preserved ejection fraction. *Nature*, *568*(7752), 351–356.

Shah, S.J.,Borlaug, B.A.,Kitzman, D.W.,McCulloch, A.D.,Blaxall, B.C.,Agarwal, R.,Chirinos, J. A., Collins, S., Deo, R. C., Gladwin, M. T., Granzier, H., Hummel, S. L., Kass, D. A., Redfield, M. M., Sam, F., Wang, T. J., Desvigne-Nickens, P., & Adhikari, B. B. (2020). Research Priorities for Heart Failure With Preserved Ejection Fraction: National Heart, Lung, and Blood Institute Working Group Summary. *Circulation*, *141*(12), 1001–1026.

Shah, S.J., Kitzman, D.W., Borlaug, B.A.,van Heerebeek, L.,Zile, M.R., Kass, D.A.,& Paulus, W. J. (2016). Phenotype-Specific Treatment of Heart Failure With Preserved Ejection Fraction: A Multiorgan Roadmap. *Circulation*, *134*(1), 73–90.

Soltani, S., Beigrezaei, S., Malekahmadi, M., Clark, C. C. T., & Abdollahi, S. (2023). Circulating levels of adropin and diabetes: a systematic review and meta-analysis of observational studies. *BMC endocrine disorders*, *23*(1), 73.

Stokar, J., Gurt, I., Cohen-Kfir, E., Yakubovsky, O., Hallak, N., Benyamini, H., Lishinsky, N., Offir, N., Tam, J., & Dresner-Pollak, R. (2022). Hepatic adropin is regulated by estrogen and contributes to adverse metabolic phenotypes in ovariectomized mice. *Molecular metabolism*, *60*, 101482.

Thapa, D., Xie, B., Manning, J. R., Zhang, M., Stoner, M. W., Huckestein, B. R., Edmunds, L. R., Zhang, X., Dedousis, N. L., O'Doherty, R. M., Jurczak, M. J., & Scott, I. (2019a). Adropin reduces blood glucose levels in mice by limiting hepatic glucose production. *Physiological reports*, *7*(8), e14043.

Thapa, D., Xie, B., Zhang, M., Stoner, M. W., Manning, J. R., Huckestein, B. R., Edmunds, L. R., Mullett, S. J., McTiernan, C. F., Wendell, S. G., Jurczak, M. J., & Scott, I. (2019b). Adropin treatment restores cardiac glucose oxidation in pre-diabetic obese mice. *Journal of molecular and cellular cardiology*, *129*, 174–178.

Thapa, D., Xie, B., Mushala, B. A. S., Zhang, M., Manning, J. R., Bugga, P., Stoner, M. W., Jurczak, M. J., & Scott, I. (2022). Diet-induced obese mice are resistant to improvements in cardiac function resulting from short-term adropin treatment. *Current research in physiology*, *5*, 55–62.

Thapa, D., Zhang, M., Manning, J. R., Guimarães, D. A., Stoner, M. W., O'Doherty, R. M., Shiva, S., & Scott, I. (2017). Acetylation of mitochondrial proteins by GCN5L1 promotes enhanced fatty acid oxidation in the heart. *American journal of physiology. Heart and circulatory physiology, 313(2), H265–H274.*

Tong D, Schiattarella GG, Jiang N, May HI, Lavandero S, Gillette TG, Hill JA. (2019). Female Sex Is Protective in a Preclinical Model of Heart Failure With Preserved Ejection Fraction. Circulation, 140(21):1769-1771.

Tong, D., Schiattarella, G. G., Jiang, N., Altamirano, F., Szweda, P. A., Elnwasany, A., Lee, D. I., Yoo, H., Kass, D. A., Szweda, L. I., Lavandero, S., Verdin, E., Gillette, T. G., & Hill, J. A. (2021). NAD^+ Repletion Reverses Heart Failure With Preserved Ejection Fraction. *Circulation research*, *128*(11), 1629–1641.

Tran, D.H., May, H.I., Li, Q. *et al.* (2020) Chronic activation of hexosamine biosynthesis in the heart triggers pathological cardiac remodeling. *Nat Commun* **11**, 1771.

Umapathi, P., et al. Excessive O-GlcNAcylation Causes Heart Failure and Sudden Death. Circulation 143, 1687-1703 (2021). 154. Tran, D.H., et al. Chronic activation of hexosamine biosynthesis in the heart triggers pathological cardiac remodeling. Nature Communications 11, 1771 (2020). 155.

Wong, C. M., Wang, Y., Lee, J. T., Huang, Z., Wu, D., Xu, A., & Lam, K. S. (2014). Adropin is a brain membrane-bound protein regulating physical activity via the NB-3/Notch signaling pathway in mice. *The Journal of biological chemistry*, *289*(37), 25976–25986.

Yang, C., DeMars, K. M., & Candelario-Jalil, E. (2018). Age-Dependent Decrease in Adropin is Associated with Reduced Levels of Endothelial Nitric Oxide Synthase and Increased Oxidative Stress in the Rat Brain. *Aging and disease*, *9*(2), 322–330.

Ye, B., Bradshaw, A. D., Abrahante, J. E., Dragon, J. A., Häußler, T. N., Bell, S. P., Hirashima, F., LeWinter, M., Zile, M. R., & Meyer, M. (2023). Left Ventricular Gene Expression in Heart Failure With Preserved Ejection Fraction-Profibrotic and Proinflammatory Pathways and Genes. Circulation. Heart failure, 16(8), e010395.

Zhu, W. Z., Palazzo, T., Zhou, M., Ledee, D., Olson, H. M., Paša-Tolić, L., & Olson, A. K. (2022). First comprehensive identification of cardiac proteins with putative increased O-GlcNAc levels during pressure overload hypertrophy. *PloS one*, *17*(10), e0276285.

ACKNOWLEDGEMENTS

This work was supported by: National Institute of Health Fellowships (F31DK134089 and T32HL110849) to B.A.S.M; National Institute of Health Shared Instrumentation Grants (S10OD023402, S10OD032141) to S.L.G.; National Institutes of Health Research Grants (R01HL124021, R01HL122596, R01HL151228) to S.Y.C.; National Institute of Health Research Grants (R01HL147861, R0HL156874) and American Heart Association Established Investigator Award (23EIA1037834) to I.S. The University of Pittsburgh Center for Metabolism and Mitochondrial Medicine is supported by the Pittsburgh Foundation (MR2020 109502) grant to M.J.J. This project used the University of Pittsburgh Medical Center (UPMC) Hillman Cancer Center and Tissue and Research Pathology/Pitt Biospecimen Core shared resource, which is supported in part by award P30CA047904. Echocardiography was carried out by the University of Pittsburgh Rodent Ultrasonography Core, which received funding from the NIH Shared Instrumentation Grant Program (S10OD023684).

AUTHOR CONTRIBUTIONS

B.A.S.M., M.J.J., and I.S. conceived the study and designed experiments. E.S.G., Y.A.A. and S.Y.C. provided essential biological samples. B.A.S.M, M.W.S., B.M., A.M.V., and S.J.M. performed experiments. B.A.S.M., B.M., S.J.M. and I.S. analyzed data. B.A.S.M. and I.S. prepared figures. J.R.M., P.B., N.B., M.S.S., S.S.S., B.A.K., C.Z., E.S.G, S.Y.C., and S.L.G provided critical input and expertise. B.A.S.M and I.S. drafted the manuscript. B.A.S.M. and I.S. edited and revised the manuscript. All authors approved the final submission.

DISCLOSURES

S.Y.C. has served as a consultant for Merck, Janssen, and United Therapeutics. S.Y.C. is a director, officer, and shareholder in Synhale Therapeutics. S.Y.C. has held grants from Bayer and United Therapeutics. I.S. is listed as the inventor on patent applications for the use of Adropin in the detection and treatment of cardiometabolic disease.

FIGURES

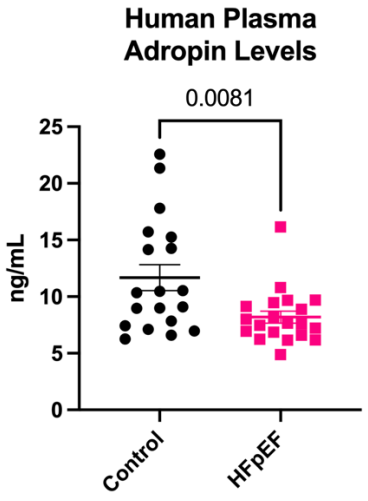

Figure 1: Adropin plasma concentration in age- and gender-matched human control and HFpEF patients. Total circulating Adropin levels in control and HFpEF patients. N = 19-20.

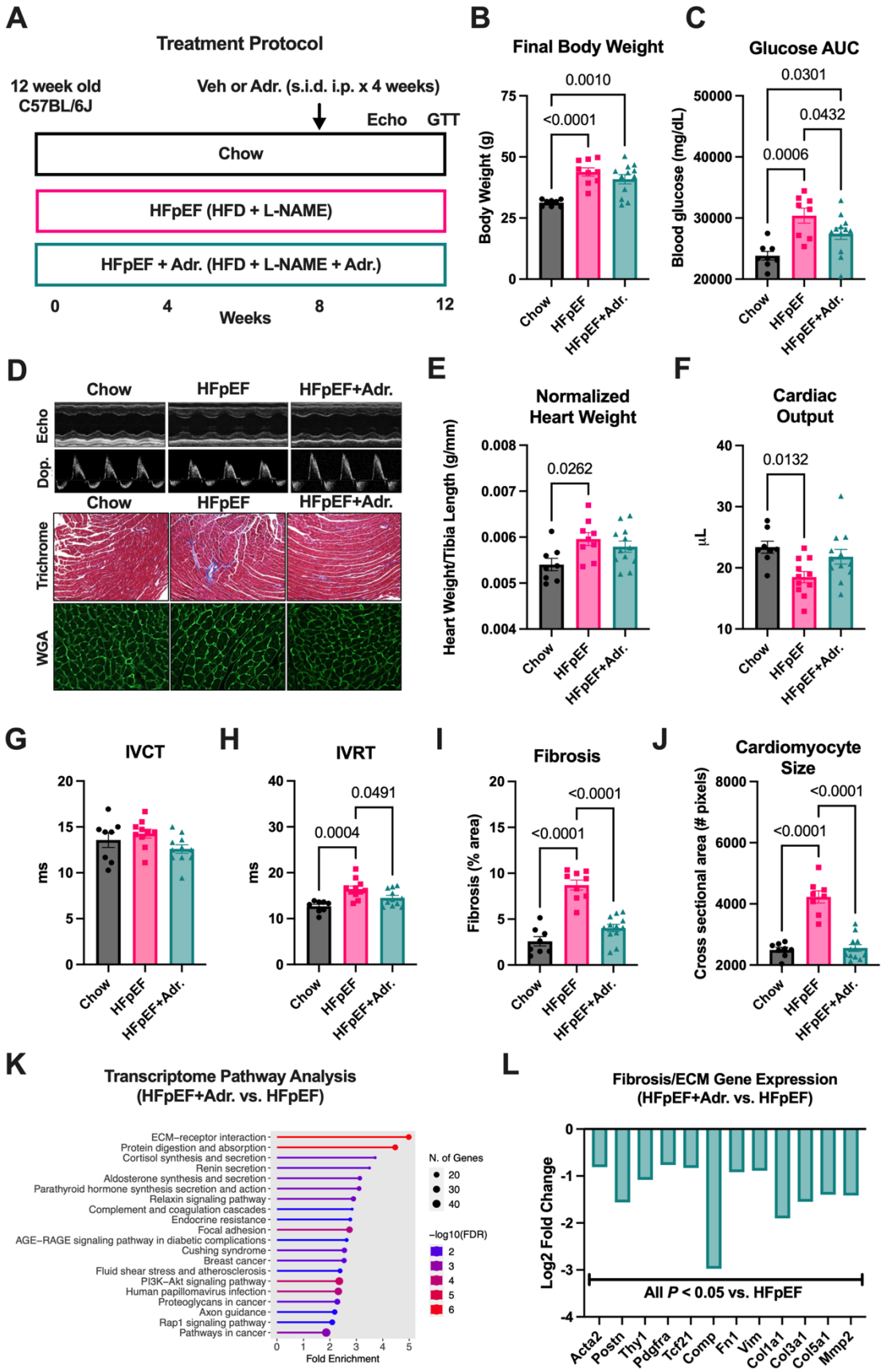

Figure 2: Recombinant Adropin treatment prevents cardiac dysfunction in a mouse model of HFpEF. A. Timeline and treatment protocol used in mouse HFpEF studies. B. Final body weight of

mice. N = 8-12. C. IPGTT glucose under-the-curve (AUC). N = 8-12. D. Representative echocardiography (M-mode and Doppler) and histology images (Masson's Trichrome and WGA). N = 8-12. E. Final heart weight normalized to tibia length. N = 8-12. F. Cardiac output. N = 8-12. G. Isovolumetric contraction time (systolic function). N = 8-12. H. Isovolumetric relaxation time (diastolic function). N = 8-12. I. Cardiac interstitial fibrosis. N = 8-12. J. Cardiomyocyte cross-sectional area. N = 8-12. K. Bulk RNA-seq pathway analysis of mouse hearts using ShinyGO in HFpEF vs. HFpEF+Adr. mice. N = 4. L. Fibrosis/ECM gene expression (fold change) in HFpEF vs. HFpEF+Adr. mice. N = 4.

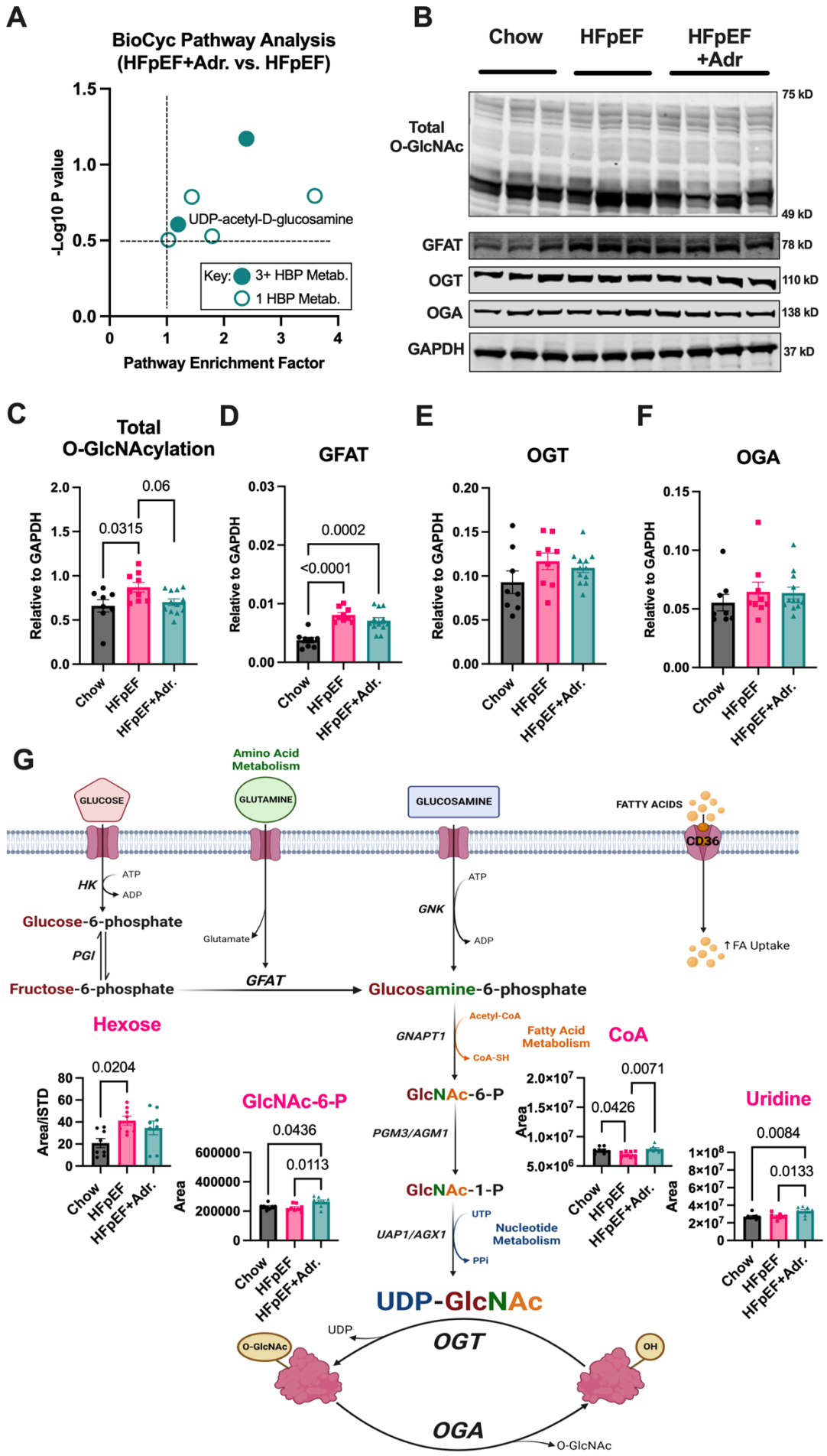
A
BioCyc Pathway Analysis
(HFpEF+Adr. vs. HFpEF)
-Log10 P value
Pathway Enrichment Factor
UDP-acetyl-D-glucosamine
Key: 3+ HBP Metab.
1 HBP Metab.
B
Chow
HFpEF
HFpEF +Adr
Total O-GlcNAc
GFAT
OGT
OGA
GAPDH
75 kD
49 kD
78 kD
110 kD
138 kD
37 kD
C
Total O-GlcNAcylation
D
GFAT
E
OGT
F
OGA
Relative to GAPDH
0.0315
0.06
0.0002
<0.0001
Chow
HFpEF
HFpEF+Adr.
G
Amino Acid Metabolism
GLUCOSE
GLUTAMINE
GLUCOSAMINE
FATTY ACIDS
CD36
HK
ATP
ADP
Glucose-6-phosphate
PGI
Fructose-6-phosphate
Glutamate
GFAT
GNK
Glucosamine-6-phosphate
↑FA Uptake
Hexose
Acetyl-CoA
GNAPT1
CoA-SH
Fatty Acid Metabolism
CoA
GlcNAc-6-P
PGM3/AGM1
GlcNAc-1-P
UAP1/AGX1
UTP
PPi
Nucleotide Metabolism
Uridine
Area/ISTD
Area
0.0204
0.0436
0.0113
0.0426
0.0071
0.0084
0.0133
UDP-GlcNAc
UDP
OGT
OGA
O-GlcNAc
OH

Figure 3: Adropin treatment limits cardiac protein O-GlcNAcylation in HFpEF mice. A. BioCyc pathway analysis of untargeted metabolites in HFpEF vs. HFpEF+Adr. hearts. HBP = hexosamine biosynthesis pathway. N = 8. B. Representative immunoblots of total cardiac O-GlcNAcylation and HBP pathway proteins. N = 8-12. C-F. Quantification of immunoblots in B. N = 8-12. G. Hexosamine biosynthesis/O-GlcNAcylation pathway metabolites. N = 8.

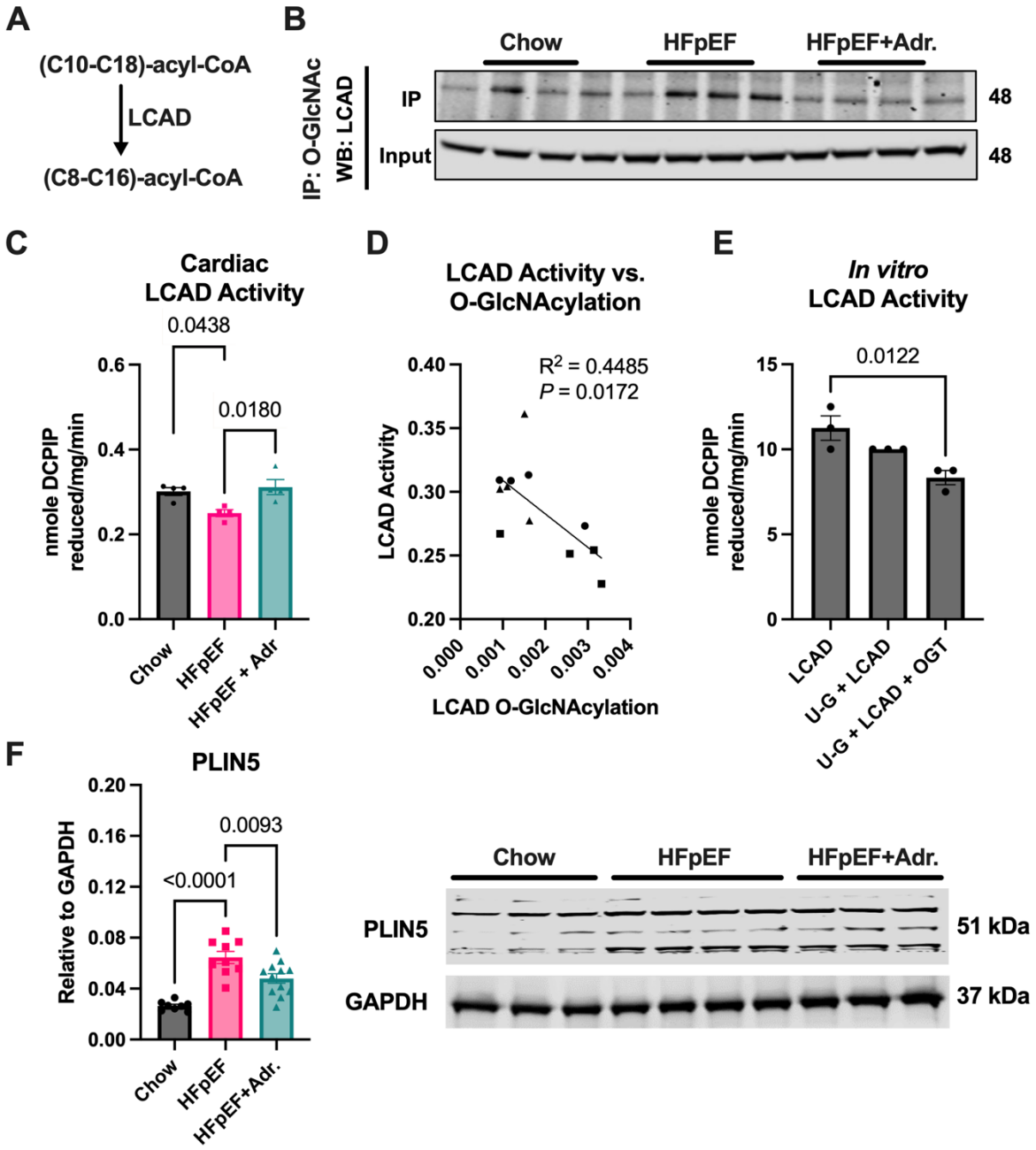

Figure 4: Adropin-mediated reductions in LCAD O-GlcNAcylation improve its enzymatic activity. A. Enzymatic function of LCAD. B. Immunoprecipitation analysis of LCAD O-GlcNAcylation status, N = 4. C. LCAD enzymatic activity from bulk cardiac tissue, N = 4. D. N = 4 per group. Circles = chow mice, squares = HFpEF mice and triangles = HFpEF+Adr. mice. E. *In vitro* enzymatic activity of recombinant LCAD after exposure to O-GlcNAcylation substrate (UDP-GlcNAc; U-G) and/or recombinant O-GlcNAc transferase (OGT), N = 3. F. Immunoblot analysis of cardiac perilipin-5 (PLIN5) abundance, N = 8-12.

SUPPLEMENTAL TABLES AND FIGURES

Control					HFpEF				
ID	**Age**	**Gender**	**Race**	**Ethnicity**	**ID**	**Age**	**Gender**	**Race**	**Ethnicity**
758	78	M	W	NH/NL	166	77	M	W	NH/NL
843	61	F	W	NH/NL	434	58	F	W	NH/NL
854	77	M	W	NH/NL	442	76	M	W	NH/NL
872	75	F	W	NH/NL	445	72	F	W	NH/NL
884	73	F	W	NH/NL	459	72	F	W	NH/NL
909	75	F	W	NH/NL	462	74	F	W	NH/NL
933	56	F	W	NH/NL	466	58	F	W	NH/NL
935	72	M	W	NH/NL	470	74	M	W	NH/NL
896	62	F	W	NH/NL	476	59	F	W	NH/NL
958	65	F	W	NH/NL	482	65	F	W	NH/NL
930	63	F	W	NH/NL	492	68	F	W	NH/NL
946	45	M	W	NH/NL	499	46	M	W	NH/NL
947	72	F	W	NH/NL	514	74	F	W	NH/NL
974	66	M	W	NH/NL	562	69	M	W	NH/NL
1137	59	F	W	NH/NL	576	70	F	W	NH/NL
992	74	M	W	NH/NL	583	63	F	W	NH/NL
1014	73	F	W	NH/NL	633	71	M	W	NH/NL
1122	50	M	W	NH/NL	636	74	F	W	NH/NL
1052	72	M	W	NH/NL	663	48	M	W	NH/NL
					675	72	M	W	NH/NL

Supplemental Table 1 – Control and HFpEF Patient Characteristics. M = male, F = female, W = white, NH/NL = non-Hispanic/non-Latino. N = 19-20.

	Chow	HFpEF	HFpEF+Adr.
LV Mass	128.6 ± 18.05	157.8 ± 25.15*	149.8 ± 24.26
Heart Rate	491.9 ± 28.93	448.1 ± 37.75	488.3 ± 42.43
Ejection Fraction (%)	64.70 ± 3.326	62.16 ± 3.941	63.73 ± 6.176
E/e'	21.66 ± 3.249	26.09 ± 5.871	27.01 ± 5.694
E/A	1.601 ± 0.2996	1.699 ± 0.3553	1.562 ± 0.3157
IVCT	13.58 ± 2.293	14.28 ± 1.511	12.60 ± 1.528
IVRT	12.67 ± 1.259	16.44 ± 2.118*	14.52 ± 1.801#
Stroke Volume	47.79 ± 7.432	41.89 ± 8.713	45.01 ± 9.634
Cardiac Output	23.38 ± 2.799	18.58 ± 3.167*	21.82 ± 4.132
LV AW; sys	1.401 ± 0.06618	1.548 ± 0.1178*	1.490 ± 0.1205
LV AW; dia	0.8807 ± 0.06180	1.121 ± 0.1100*	1.035 ± 0.1213*
LV PW; sys	1.211 ± 0.1044	1.255 ± 0.1376	1.312 ± 0.1653
LV PW; dia	0.7841 ± 0.1113	0.8945 ± 0.07463	0.8639 ± 0.1161
LV MPI (Tau)	0.5290 ± 0.03861	0.6154 ± 0.08687*	0.5330 ± 0.06274#
LAA	4.909 ± 0.4121	4.788 ± 0.7369	5.002 ± 0.6408

Supplemental Table 2 – Echocardiography analysis of Chow, HFpEF, and HFpEF+Adr. mice. LV = left ventricle; IVCT = isovolumetric contraction time; IVRT = isovolumetric relaxation time; AW = anterior wall; PW = posterior wall; MPI = myocardial performance (Tau) index; LAA = left atrial area; sys = systolic; dia = diastolic; * = $P < 0.05$ vs. Chow; # = $P < 0.05$ vs. HFpEF.

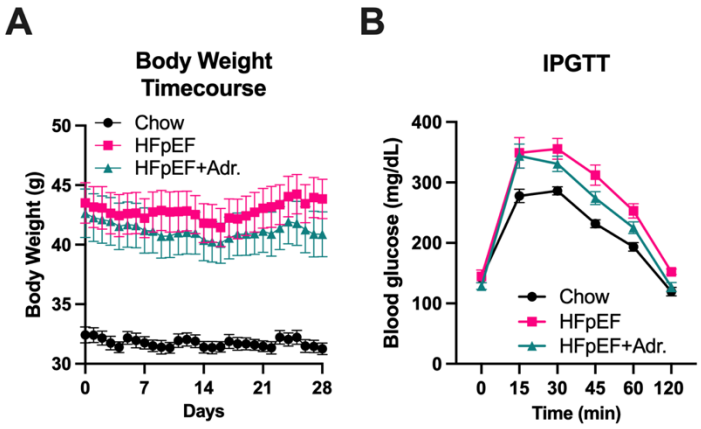

Supplemental Figure 1: Body weight and IPGTT timecourse data. N = 8-12.

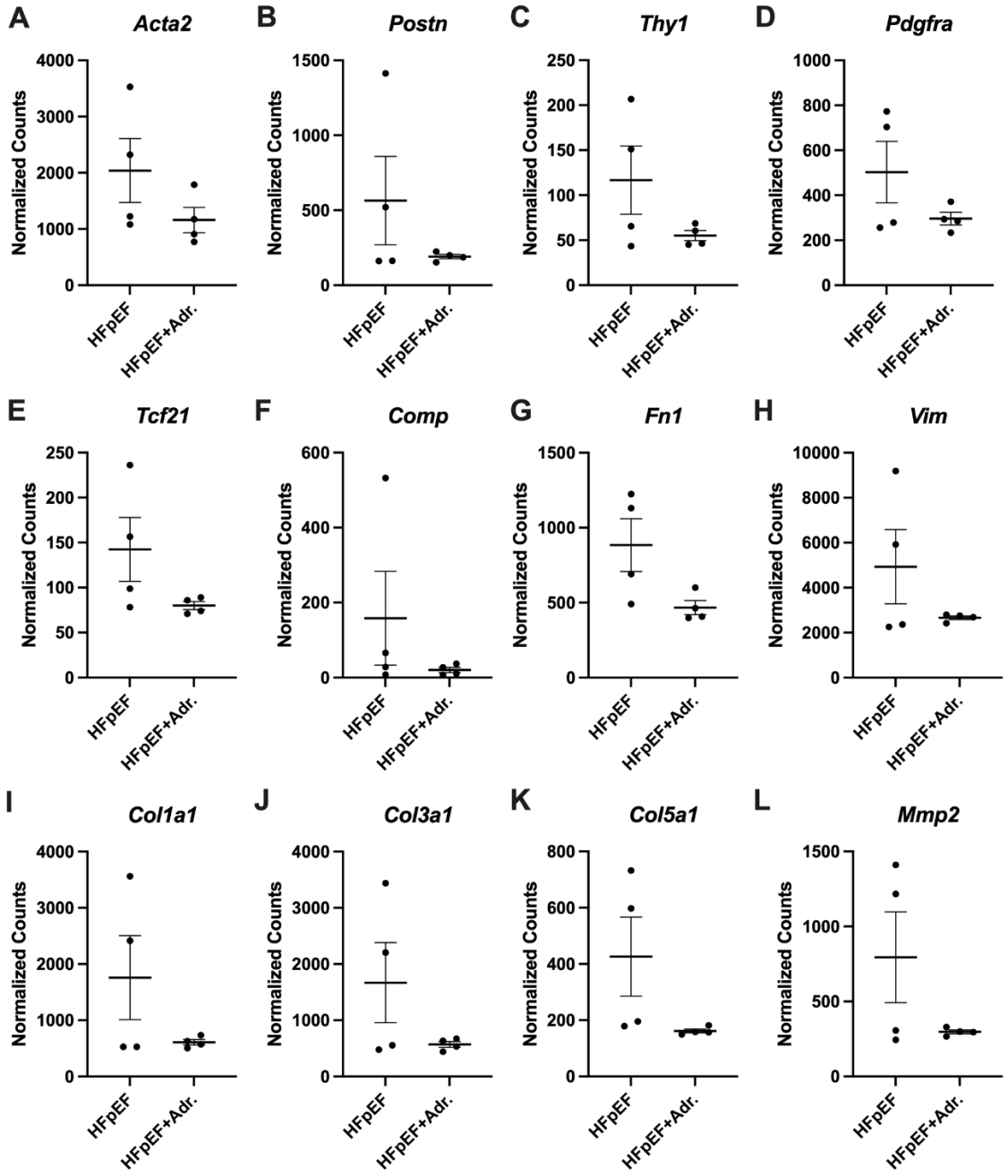

Supplemental Figure 2: Bulk RNA-seq measurements of ECM/Fibrosis genes. N = 4.

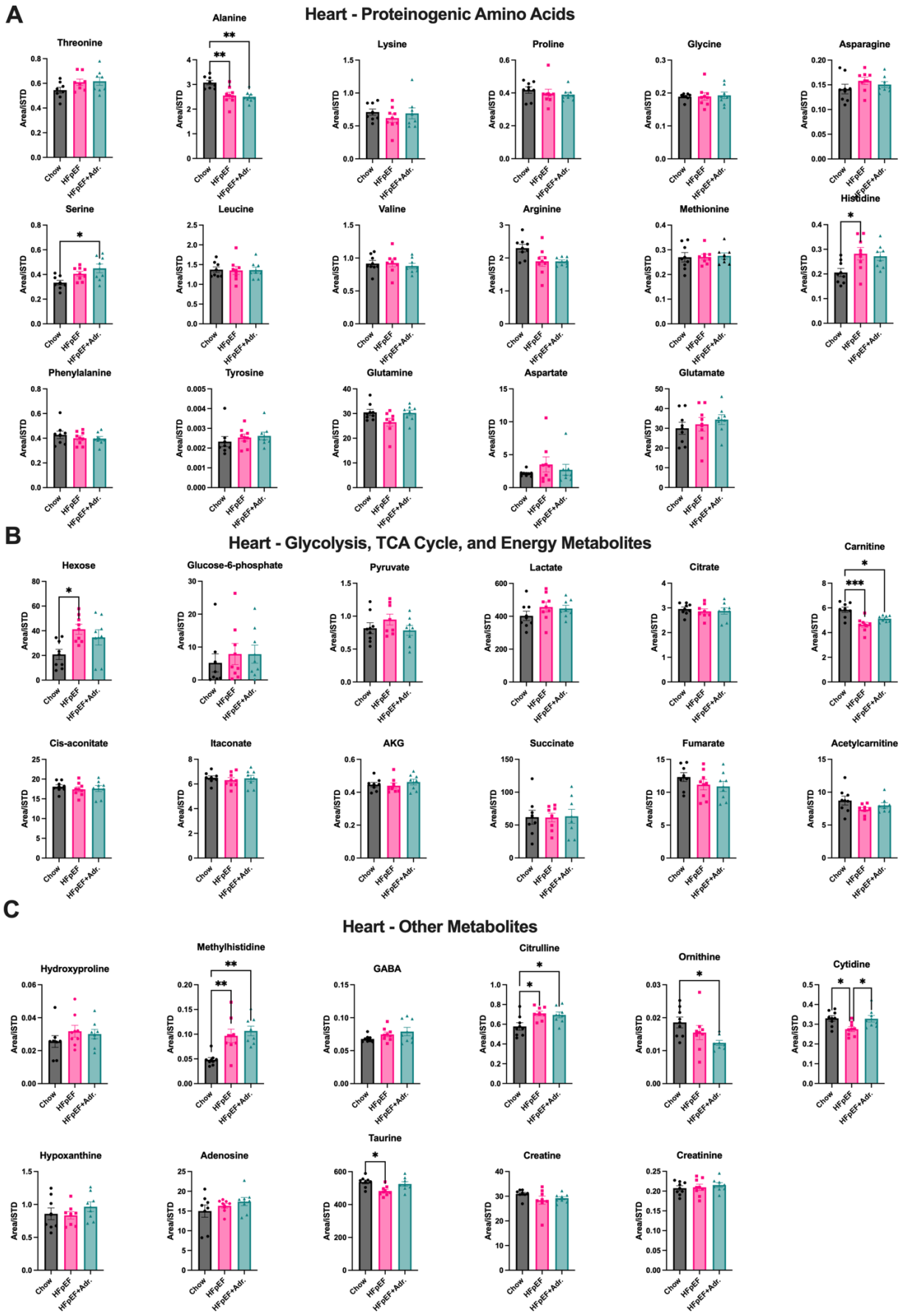

Supplemental Figure 3: Heart targeted metabolomics. N = 8, * = $P < 0.05$, ** = $P < 0.01$.

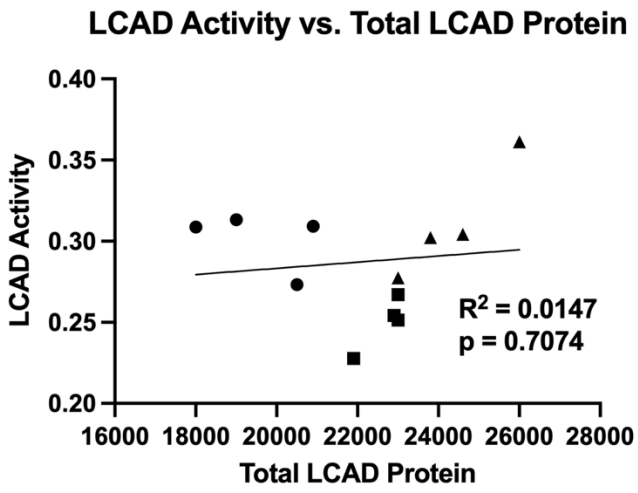

Supplemental Figure 4: Correlation between LCAD activity and enzyme abundance. N = 4 per group. Circles = chow mice, squares = HFpEF mice and triangles = HFpEF+Adr. mice.

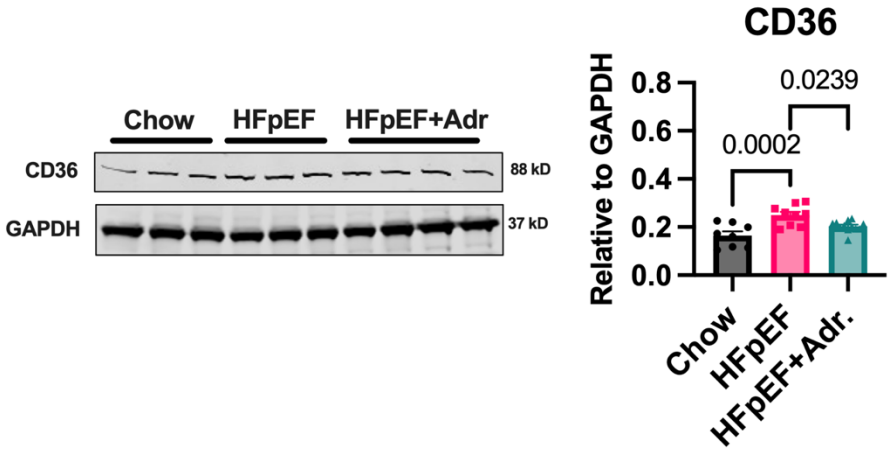

Supplemental Figure 5: Cardiac CD36 protein abundance. N = 8-12. N.B. The same membrane was used as in Figure 3, and therefore the same GAPDH loading control image is used here.